Chaotic Lagrangian Motion on a Rotating Sphere

Vered Rom-Kedar[1], Yona Dvorkin[2] and Nathan Paldor[2].

[1] The Department of Applied Mathematics and Computer Science, The Weizmann Institute of Science, P.O.B. 26, Rehovot 76100, Israel.

[2] The Department of Atmospheric Sciences, The Hebrew University of Jerusalem, Jerusalem 91904, Israel.

Abstract: We study the motion of Lagrangian particles launched on a geopotential surface of a rotating sphere (e.g. floats in the deep ocean) where the latter is zonally perturbed by some travelling pressure wave (e.g. tidal waves). The motion of these particles is described by a near integrable, two-degrees-of-freedom Hamiltonian system. For some regions in parameter and phase space, the system may be reduced to a one-and-a-half-degrees-of-freedom Hamiltonian system and standard tools may be applied to prove the existence of chaotic homoclinic behavior, hence of the phenomena of anomalous transport associated with the homoclinic chaos. In other regions zonally localized structures and homoclinic tangles with back-flows, associated with the three dimensionality of the energy surfaces appear, as well as resonant behavior of unstable periodic orbits.

1. Introduction

The simplest possible two-dimensional motion on a rotating sphere, due only to Coriolis force (i.e. in the absence of any body force), is called the inertial motion. It may be relevant for describing the motion of Lagrangian ("passive") particles in the atmosphere (such as weather balloons, pollutants or satellites in the upper atmosphere) or for describing the motion of floats in the deep ocean. Each of these applications involves different scales of velocities, and various simplifying assumptions on the dynamics which need to be carefully examined (in particular, for the atmospheric applications the role of the interaction of changes in pressure and particle velocity). In the context of atmospheric and oceanographic flows, the possible solutions of the inertial (i.e. force free) motion have been described in various textbooks[1] for some specific cases (e.g. small latitudinal extent). The introduction of the general equations of motion (namely when the scale of the motion is allowed to encompass the entire globe), their integrals, and the full analysis of their possible solutions has been introduced only recently by Paldor and Killworth[2]. The influence of weak zonally travelling pressure waves, perturbing the geopotential surface from its mean spherical shape, was considered by Paldor and Boss[3]. They have demonstrated that chaotic trajectories exist and cause dispersion of lines of Lagrangian particles. In fact, many different waves exist in the real atmosphere - tidal (thermal or planetary) waves are examples of eastward propagating waves while Rossby waves propagate westward. The effect of these two waves on particle dispersion will be shown to be qualitatively different. Here we set the ground for a complete analysis of these equations, and include results regarding mixing and transport for some particularly simple cases. We concentrate on the mathematical aspects of the analysis, and at this point, use the physical circumstance as a motivation for posing the mathematical problems. The application of our results to observations on the physical system is deferred to a follow-up study.

Mathematically, the equations we consider are near integrable two-degrees-of-freedom Hamiltonian system. Most of our conclusions are based upon known results from various works in dynamical system theory. The use of several different tools in understanding one system seems to be unique, and brings up the issue of matching between the different techniques in the intermediate regimes. The new concept/method we introduce here is the representation of colored energy surfaces: we plot a two dimensional cross-section of the three dimensional energy surfaces and tag them according to the behavior of the angular variable. This geometrical representation enables an immediate interpretation of the generic qualitative behavior and aids in identifying the occurrence of all singular behavior.

It has been observed that the chaotic zone in two- and four-dimensional area preserving maps which is associated with the existence of homoclinic tangles exhibits anomalous transport in which Levỳ flights alter the decay rate of the autocorrelators and lead to non-diffusive behavior[4]. Moreover, such a behavior has been observed experimentally in a rotating system in which the inertial motion may be realized (see Weeks et al., this proceeding). The analysis of our system reveals the existence of homoclinic chaos of various types, with two types which are "generic" - the usual homoclinic tangle associated with one-and-a-half d.o.f. Hamiltonian systems and a homoclinic tangle with a back-flow in the angular direction. It follows that the phenomena of anomalous transport is present in our system in the former case. The appearance of the Lèvy flights in the second case is yet to be explored.

This paper is organized as follows: in section 2 we describe the structure of the integrable system and its symmetries. In section 3 we construct the energy surfaces and present the division to the parameter ranges according to the expected behavior under perturbation. In section 4 we present the Melnikov analysis results for the simplest, infinite wave length perturbation case. We discuss the implication of this result on maximal mixing and maximal chaotic zone.

2. The phase space geometry

The non-dimensional Lagrangian momentum equations for the eastward and northward velocity components (u, v) and the rate of change of the longitude and latitude coordinates (λ, ϕ) are given by:

$$\frac{d\lambda}{dt} = \frac{u}{\cos\phi} \tag{2.1a}$$

$$\frac{du}{dt} = v\sin\phi(1+\frac{u}{\cos\phi}) - k\epsilon\frac{A(\phi)}{\cos\phi}\cos(k\lambda-\sigma t). \tag{2.1b}$$

$$\frac{d\phi}{dt} = v \tag{2.1c}$$

$$\frac{dv}{dt} = -u\sin\phi(1+\frac{u}{\cos\phi}) - \epsilon A'(\phi)\sin(k\lambda-\sigma t) \tag{2.1d}$$

Equations (2.1) have been nondimensionalized using the radius of the earth for length scale and twice the frequency of the earth's rotation for the frequency scale, so that a nondimensional time unit corresponds to $24h/2\pi \approx 1.901$ hours. Order one velocities in the nondimensional variables turn out to be nearly 1 km/second dimensional velocities, so the relevant nondimensional velocities for atmospheric flows are of order 0.01 , For satellites, the relevant scales are of order 1 and for oceanographic flows of order 0.001. $A(\phi)$ represents the latitude dependent amplitude of a pressure wave (divided by the density), which is assumed to be even:

$$A(\phi) = A(-\phi) \quad A(0) = 1, \quad A'(0) = 0. \tag{2.2}$$

$A(\phi)$ may represent, for example, the amplitude of a daily tidal forcing ($k = 1, \sigma = 1$), for which the amplitude $A(\phi)$ may be either taken as constant ($A(\phi) = 1$) or to vary with latitude like $A(\phi) = \cos^3\phi$, see Paldor and Boss[3] for discussion. Higher or negative wavenumbers may be associated with other waves present in the atmosphere (e.g. Rossby waves). For the atmospheric flows the relevant scale for the pressure wave is that of the order of the kinetic energy, namely ϵ is $O(10^{-4})$. Finally, we note that the polar coordinates introduce apparent singularity at the poles; $\cos\phi = 0$ there, but u vanishes there as well, so no real singularity is encountered when the solutions pass near the poles.

When no waves are present the motion is integrable; Two integrals of motion were derived in Paldor and Killworth[2] for the inertial trajectories, corresponding to the angular momentum D and the kinetic energy E:

$$D = \cos\phi(\cos\phi + 2u) \tag{2.3a}$$

$$E = u^2 + v^2. \tag{2.3b}$$

Using (2.3a) u may be expressed in terms of D and ϕ:

$$u = \tfrac{1}{2}(\tfrac{D}{\cos\phi} - \cos\phi) \tag{2.4}$$

When $\epsilon = 0$ the equation for λ decouples, D is conserved so it is considered a parameter, and the phase flow of the two dimensional system obtained for (ϕ, v) depends on the value of D as follows:

When $|D| > 1$ the origin is stable (elliptic) and is surrounded by periodic orbits which visit both hemispheres. Denote the maximal latitude reached by a periodic orbit by $\phi_{\max} = \phi_{\max}(E, D)$.

When $|D| < 1$ the origin is unstable (hyperbolic) and two stable, elliptic fixed points are created at

$$(\phi_{ell}, v_{ell}) = \pm(\arccos\sqrt{|D|}, 0). \tag{2.5}$$

The origin has two homoclinic orbits†, one in each hemisphere: $q_h^{\pm}(t;\phi_{hmax}) = \pm(\phi_h(t;\phi_{hmax}), v_h(t;\phi_{hmax}))$ where ϕ_{hmax} is the maximal latitude reached by the homoclinic orbit and is given by

$$\cos\phi_{hmax} = |D|. \tag{2.6}$$

While not included here for lack of space, we note that Eqs. (2.1) provide example in which all unperturbed solutions may be found analytically - the homoclinic orbits to the origin $q_h(t;\phi_{hmax})$ for $|D| < 1$, the associated homoclinic solution for the longitude position $\lambda_h^{\pm}(t;\phi_{hmax})$, the period of the periodic orbits in ϕ, $P_\phi(\phi_{\max};\phi_{hmax}) = P_\phi(E, D)$ and the longitude position after completion of one period in the ϕ variable. In particular, exact predictions for the location of resonances may be found easily.

The homoclinic orbits separate the phase space to three distinct regions - regions R_1 and R_2 contain periodic orbits which are restricted to one hemisphere (north and south respectively) whereas region R_3 contains periodic orbits with $\phi_{\max} > \phi_{hmax}$. The area of the bounded regions is:

$$\mu(R_1(\phi_{hmax})) = \mu(R_2(\phi_{hmax})) = \sin\phi_{hmax} - \phi_{hmax}\cos\phi_{hmax}. \tag{2.7}$$

It follows from (2.1) that when $\epsilon \neq 0$

$$\tfrac{dD}{dt} = -2\epsilon A(\phi)k\cos(k\lambda - \sigma t), \tag{2.8}$$

hence there is a major difference between the $k = 0$ and $k \neq 0$ cases:

Forcing with infinite wavelength ($k = 0$):

This forcing corresponds to a perturbation which does not vary with longitude. If the amplitude of the pressure wave is independent of latitude ($A(\phi) = const.$) then the perturbation merely changes periodically the radii of the spherical geopotential and hence has no effect on the motion along it. Thereby, only latitude dependent amplitude ($A'(\phi) \neq 0$) is of interest. Since the angular momentum is conserved in this case, using (2.4) it follows that equations (2.1c ,2.1d) are independent of λ and may be analyzed using the standard tools of a one-and-a-half degrees of freedom Hamiltonian system, depending on the

† These are solutions which are asymptotic to the origin as $t \to \pm\infty$.

parameters D, σ and on $A'(\phi)$:

$$\frac{d\lambda}{dt} = \frac{1}{2}(\frac{D}{\cos^2\phi} - 1) \tag{2.9a}$$

$$\frac{dD}{dt} = 0 \tag{2.9b}$$

$$\frac{d\phi}{dt} = v \tag{2.9c}$$

$$\frac{dv}{dt} = \frac{1}{8}\sin(2\phi)(1 - \frac{D^2}{\cos^4\phi}) + \epsilon A'(\phi)\sin(\sigma t) \tag{2.9d}$$

and the Hamiltonian:

$$H(\phi, v, t; D) = \tfrac{v^2}{2} + \tfrac{1}{8}(\tfrac{D}{\cos\phi} - \cos\phi)^2 - \epsilon A(\phi)\sin(\sigma t). \tag{2.10}$$

The equations and Hamiltonian written for $k = 0$ clearly demonstrate the relevance of the restriction to latitude dependent amplitude of the perturbation. More details regarding this case are presented in section 4.

Forcing with finite wavelength ($k \neq 0$):

Introducing the wave velocity c:

$$c = \tfrac{\sigma}{k} \tag{2.11}$$

and defining θ, the conjugate variable of D, by:

$$\theta = \tfrac{1}{2}(\lambda - ct), \tag{2.12}$$

(2.1) is replaced by:

$$\frac{d\theta}{dt} = \frac{1}{4}\frac{D}{\cos^2\phi} - \tfrac{1}{2}(c + \tfrac{1}{2}) = \frac{\partial H}{\partial D} \tag{2.13a}$$

$$\frac{dD}{dt} = -2k\epsilon A(\phi)\cos(2k\theta) = -\frac{\partial H}{\partial\theta} \tag{2.13b}$$

$$\frac{d\phi}{dt} = v = \frac{\partial H}{\partial v} \tag{2.13c}$$

$$\frac{dv}{dt} = \frac{1}{8}\sin(2\phi)(1 - \frac{D^2}{\cos^4\phi}) - \epsilon A'(\phi)\sin(2k\theta) = -\frac{\partial H}{\partial\phi}, \tag{2.13d}$$

where H is the Hamiltonian given by:

$$H(\phi, v, \theta, D) = \tfrac{v^2}{2} + \tfrac{1}{8}(\tfrac{D}{\cos\phi} - \cos\phi)^2 - \tfrac{c}{2}D + \epsilon A(\phi)\sin(2k\theta). \tag{2.14}$$

Using the symmetries of (2.13) , it is easy to show that the relevant parameters ranges for (2.13) are:

$$k > 0, \qquad \epsilon \geq 0, \qquad -\tfrac{1}{2} \leq c < \infty, \tag{2.15}$$

as all other values may be reduced to the above. Mathematically, the natural period for θ is π/k, however, physically, it is π. When considering dispersion of particles, this distinction is important, hence we keep $\theta \in [0, \pi)$. By the evenness of $A(\phi)$, the Poincaré map in θ at θ_0 is symmetric with respect to:

i. $\phi \to -\phi, \quad v \to -v$ for all θ_0.

ii. $\phi \to -\phi, \theta \to -\theta, t \to -t$ when $\theta_0 = j\pi/2k + \pi/4k$ for some integer j.

However, (2.13) is *not symmetric* with respect to reflections in D: when $D \to -D$ the equation for θ changes in a non invariant manner (though for the unperturbed case, the system in (ϕ, v) is symmetric with respect to reflections in D). This asymmetry is due to the unidirectional rotation of the earth.

3. The Energy Surfaces

Equations (2.13) constitute a weakly coupled two-degrees-of-freedom Hamiltonian system, so their solutions lie on three dimensional energy surfaces in (v, ϕ, D, θ) phase space, given by level sets of H of (2.14). The structure of the energy surface serves as a backbone for understanding the solution structure in the different regions of parameter and phase space.

Below, the construction of the energy surfaces for $c > 0$ (Figure 1) and $c < 0$ (Figure 2) is described. Then we discuss the implications of the surface structure on the dynamical behavior in the different regimes in phase space and the analysis of these regimes.

3.1 Construction of the Energy Surfaces

We construct the surfaces at the cross-section $\theta = 0$, so that the $O(\epsilon)$ term vanishes. The actual energy surfaces are three dimensional, and may be represented symbolically as the cross-sections presented in Figure 1 or Figure 2, multiplied by a circle on which the variable θ varies. Other cross-sections on the circle, corresponding to different values of θ may be viewed as changing the value of H by an $O(\epsilon)$ amount and as slight deformation of the surface if $A(\phi)$ is not constant. This effect is especially significant near values of H for which the singularities of the energy surface change.

To present the motion in the θ direction in a compact fashion we color the regions on the energy surface for which $\frac{d\theta}{dt}$ is positive along the unperturbed orbits by light shading and the regions on which it is negative by dark shading. This coloring scheme enables us to read of the structure of the four-dimensional flow from the two dimensional energy surface plot.

The energy surfaces of Figure 1 and Figure 2 are plotted for increasing values of H - picking the typical structure in each regime of H values as described below.

To find the minimal relevant H value, we use (2.14) to conclude that at the origin

$$H_o(D) = H(0,0,0,D) = \tfrac{1}{8}(D-1)^2 - \tfrac{c}{2}D, \tag{3.1}$$

Hence, the minimal value of H for which an energy surface includes the origin is given by:

$$H_{\min} = \min_D H_o(D) = -\tfrac{1}{2}c(1+c). \tag{3.2}$$

The value of D at the origin for a given H value is:

$$D_\pm(H) = (1+2c) \pm 2\sqrt{2H + c(1+c)}. \tag{3.3}$$

It follows that the minimizing D value (i.e. the value of D at H_{min}) is:

$$D_r = 1 + 2c. \tag{3.4}$$

Consider the case $c > 0$. Then, $D_+(H) > 1$ for all $H > H_{\min}$, and $D_-(H) \geq 1$ for $H \in [H_{\min}, H_{-c/2}]$ where

$$H_{-c/2} = \min_H \{D_{-\text{sign}(c)} = 1\} = -c/2. \tag{3.5}$$

From (2.14), for $\theta = 0$,

$$\tfrac{v^2}{2} = H - \tfrac{1}{8}(\tfrac{D}{\cos\phi} - \cos\phi)^2 + \tfrac{c}{2}D, \tag{3.6}$$

so, for $D \in (D_-(H), D_+(H))$ the r.h.s. of (3.6) is positive at $\phi = 0$, hence the energy surfaces for these values of H are as depicted in Figure 1 a. Moreover, for $c > 0$, (3.6) has a real solution for some D value iff $H \geq H_{\min}$ so we need not consider smaller values of H.

To color Figure 1 a, we investigate the behavior of $\frac{d\theta}{dt}$. It follows from (2.13a) that

$$\left.\tfrac{d\theta}{dt}\right|_{\phi=0} = \tfrac{1}{4}(D - 1 - 2c)$$

hence $\frac{d\theta}{dt}$ is positive at $\phi = 0$ for $D > 1 + 2c$ and negative for $D < 1 + 2c$. Moreover, $\frac{d\theta}{dt}$ changes sign when $\frac{d\theta}{dt} = 0$, and this may happen iff $\phi = \phi_r$ where

$$\cos^2\phi_r = \tfrac{D}{2c+1}. \tag{3.7}$$

Hence, $\frac{d\theta}{dt}$ may change sign along orbits only if $0 < D < D_r$ where $D_r = 1 + 2c$ as in (3.4). Substituting (3.7) (and $\epsilon = 0$) in (2.14) we restrict D so that v^2 is non-negative at $\phi = \phi_r$; since

$$v^2 = 2H + \tfrac{c(1+c)D}{1+2c},$$

and the r.h.s. vanishes for $D = D_\Delta(H)$ where

$$D_\Delta(H) = -\tfrac{2H}{c}(1 + \tfrac{c}{1+c}), \tag{3.8}$$

we find that $\frac{d\theta}{dt}$ vanishes on a given energy surface, H, for $\phi = \phi_r$ only when $D \in [\max\{0, D_\Delta(H)\}, D_r]$ for $c > 0$ and when $D \in [0, D_r]$ for $c < 0$.

It follows that for $c = 0.5$, $H_{\min} = -0.375, H_{-c/2} = -0.25$, hence Figure 1 a falls into this regime. Now we describe briefly the changes in the energy surfaces for $c > 0$ as H is further increased from its minimal value H_{min}. At $H = H_{-c/2}$, $D_-(H) = 1$, namely the bifurcation point lies on this energy surface. Increasing H further brings the separatrix and the elliptic points onto the energy surface. Equations (2.5) and (2.14) imply, in this case, that the elliptic points on the energy surface H have angular momentum:

$$D_{ell}(H) = \begin{cases} \frac{-2H}{c} & H > 0 \\ \frac{-2H}{c+1} & H < 0. \end{cases} \tag{3.9}$$

Also, equation (3.3) implies that $|D_-(H)| < 1$ for $H_{-c/2} \le H \le H_{\max}$ where

$$H_{\max} = \max_H \{H | D_-(H) \ge -1\} = H_o(-1) = \tfrac{1}{2}(c+1), \tag{3.10}$$

hence the separatrices emanating from $(0, 0, D_-(H), \theta)$ and the elliptic points are contained in the energy surface with energy H for such H values, as depicted in Figure 1 b-e.

The difference between the first three figures Figure 1 b,c,d is the different behavior of $\frac{d\theta}{dt}$ in the vicinity of the separatrices; Indeed, as long as $D_-(H) < D_\Delta(H)$, $\frac{d\theta}{dt}$ may not vanish along the separatrix, as shown in Figure 1 b. Since $D_-(H) = D_\Delta(H)$ when $\phi_r = \phi_{hmax}$, we use (2.6) and (3.7) to conclude that at that point $D_-(H) = D_\Delta(H) = D_c$, where

$$D_c = \tfrac{1}{2c+1}, \tag{3.11}$$

and this determines the critical value of H:

$$H_c = H_o(D_c) = \tfrac{1}{8}\left(\tfrac{1}{(1+2c)^2} - 1\right). \tag{3.12}$$

Hence, for $H \in (H_{-c/2}, H_c)$, $\frac{d\theta}{dt}$ is negative for all (ϕ_h, v_h) as depicted in Figure 1 b, for $H = H_c$, $\frac{d\theta}{dt}$ vanishes at one point along the separatrix, namely, at $\phi = \phi_{hmax}$, and otherwise it is negative, and for $H > H_c$, there is a region of ϕ values, $\phi_r < \phi < \phi_{hmax}$, for which $\frac{d\theta}{dt}$ is positive whereas for $\phi < \phi_r$ $\frac{d\theta}{dt}$ is negative, as shown in Figure 1 c ($H_c(c = 0.5) = -3/32 \approx 0.094$). When $H = 0$, $D_{ell} = D_\Delta(H) = 0$, corresponding to the degenerate behavior at the poles. When $0 < H < \frac{1}{8}$, $D_-(H) > 0$ and $D_{ell} < 0$, all orbits with $0 < D < 1$ have regions of back-flow where $\frac{d\theta}{dt} > 0$, while the periodic orbits with $D < 0$ have none. The intersection of the energy surface with $D = 0$ surface consists of interior orbits, corresponding to periodic motions restricted to one hemisphere, passing through the poles with $v < \frac{1}{2}$. At $H = \frac{1}{8}$ the separatrix reaches $D = 0$, connecting the equator and the poles (Figure 1 d). For $\frac{1}{8} < H$ The intersection

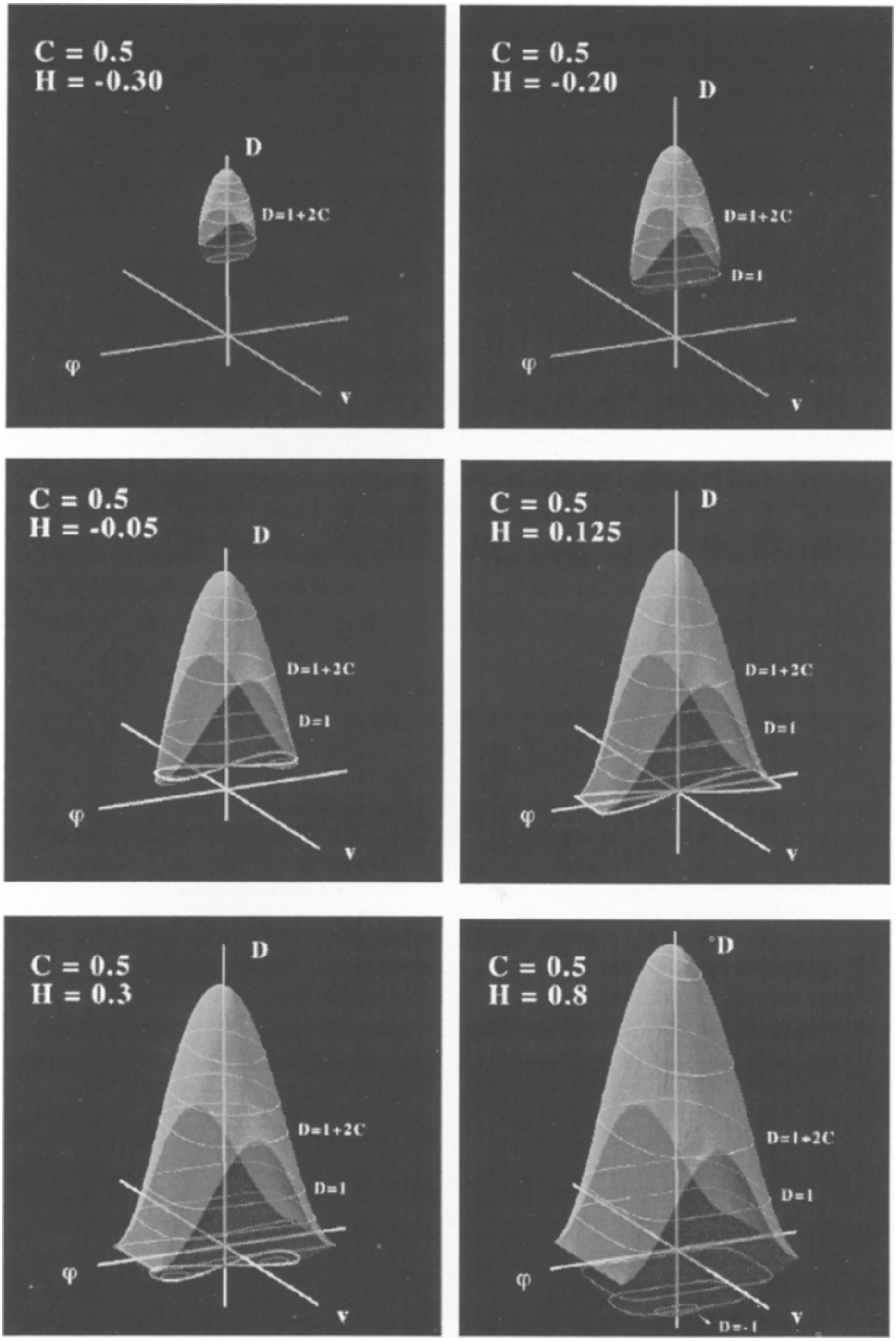

Figure 1. The energy surfaces for $c > 0, \theta = 0$.

of the energy surface with $D = 0$ surface contains exterior orbits, corresponding to periodic motions going through both hemispheres, passing through both the north and south poles with $v > \frac{1}{2}$. These motions correspond to high kinetic energies and are not expected to be encountered in observed oceanic or atmospheric flows. For $\frac{1}{8} < H < H_{\max}$ the separatrix and the elliptic points have negative angular momentum $(0 > D_{-}(H), D_{ell}(H) > -1)$ where $\frac{d\theta}{dt}$ does not change sign (Figure 1 e). When $H > H_{\max}$ the energy surface includes only exterior periodic orbits, and the periodic orbits with $0 < D < D_r$ have regions of back-flow (Figure 1 f).

Similar analysis for the $c < 0$ case results in Figure 2. Clearly new structures of the energy surface appear. Most notably, for $0 < H < H_{min}$, there exist an energy surface consisting of two connected components (Figure 2 a). At $H = H_{min}$ the two components coalesce at the origin (Figure 2 b), and for $H_{min} < H < \min\{-c/2, 0.125\}$ there exist two homoclinic orbits emanating from $D_{\pm}(H)$ with $0 < D_{\pm} < 1$ (Figure 2 c). For $0.125 < H < H_{max}$ the lower homoclinic orbit has $D_{-}(H) \in (0, -1)$ (Figure 2 d,e) whereas for $H_{min} < H < -c/2$ the upper homoclinic orbit has $D_{+}(H) \in (D_r, 1)$ (Figure 2 c,d). The behavior near $D = D_r$ for $H \approx H_{min}$ is of special interest.

3.2 Regimes of analysis:

The series of energy surfaces of Figure 1, Figure 2 and the structure of the unperturbed motion on them reveals that there are three types of typical structures which emerge for small non vanishing pressure waves. Moreover, the critical values of H and D for which a certain degenerate behavior appears arise naturally as the limiting values for which the boundary separating different subregions is approached.

Typical Structures

A. KAM surfaces: The KAM surfaces correspond, in the unperturbed case, to the motion on tori composed of the periodic motion in ϕ on the presented cross-section and the periodic motion in θ, with irrationally related period. By KAM theory, even for nonzero perturbation (yet sufficiently small) most of these tori persist. These tori are two dimensional surfaces which divide the energy surfaces, hence their persistence guarantees stability in the D direction (as is the standard case for two-degrees-of freedom systems).

B. Resonances: The coupling between the rationally related periodic motion in the angles ϕ and θ creates resonances. When $\frac{d\theta}{dt}$ is nonvanishing these resonances are necessarily of rotational nature in θ, namely θ covers the interval $[0, \pi]$. When $\frac{d\theta}{dt}$ changes sign along an orbit, (i.e. the orbits containing two-colors in Figure 1 or Figure 2) there exists the possibility of oscillatory resonance, which, under the perturbation, results in localized structures with respect to the travelling wave. Moreover, one expects that the size of these oscillatory resonances will be the most significant (in future work we plan to indicate the values of D on which strong resonances are to occur on the energy surface).

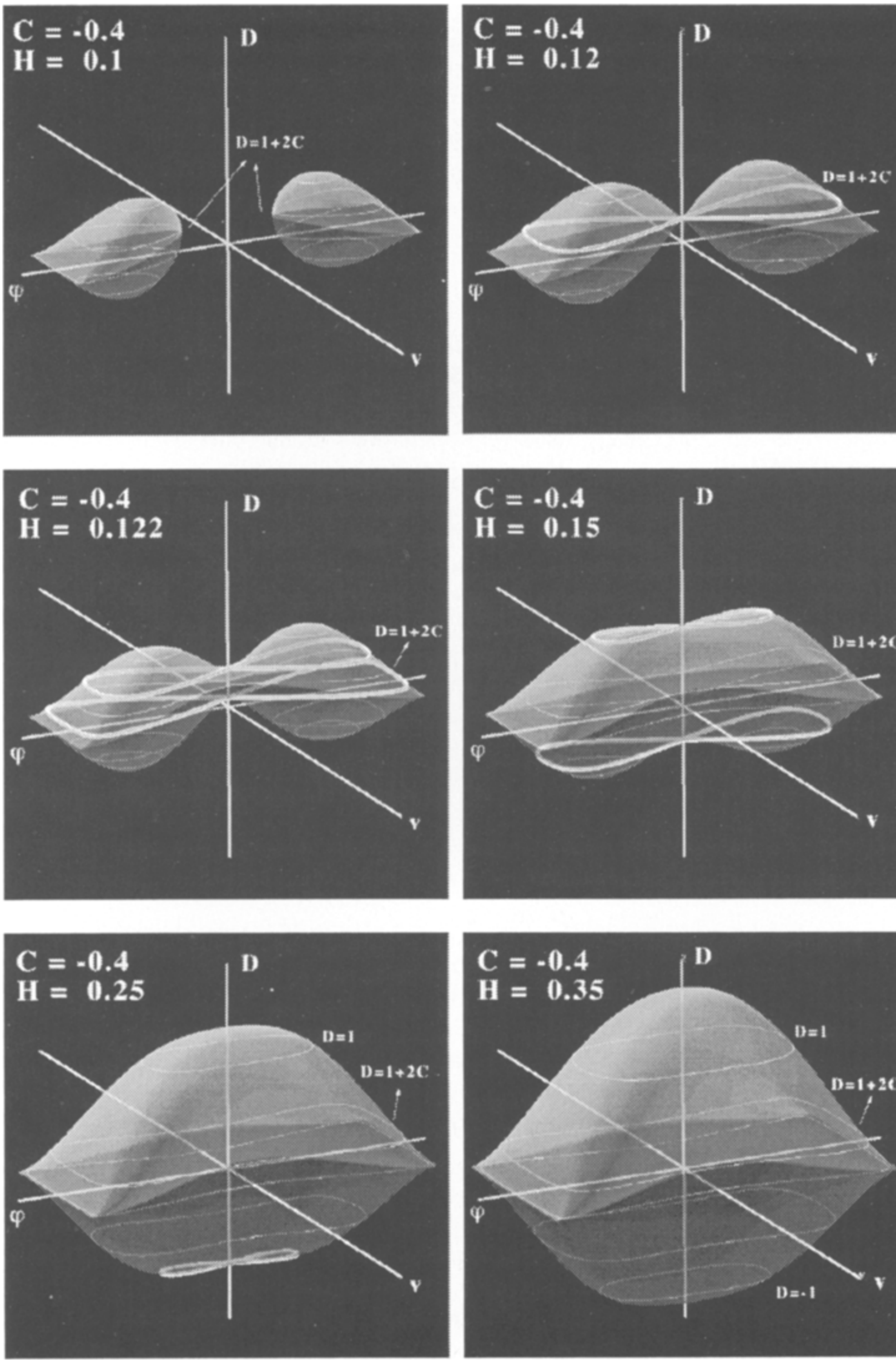

Figure 2. The energy surfaces for $c < 0, \theta = 0$.

C. Near separatrix behavior:

i. *Monotonic θ dependence:* when $\frac{d\theta}{dt}$ is bounded away from zero over an invariant region which includes the separatrix, the system (2.13) is reduced, as in Marsden and Holmes[5], to a one-and-a-half degrees-of-freedom Hamiltonian system, where θ replaces time. The reduction and the analysis of the reduced system will be presented elsewhere. From Figure 1 and Figure 2 we identify the intervals in H for which the unperturbed solutions in θ near the separatrix are monotonic in t (for these intervals the neighborhood of the separatrix has only one color shading in the figure):

I. $c > 0$:

Ia. For $H \in (-c/2, H_c)$ the component $\theta(t)$ is monotonic near the separatrix emanating from $D_-(H)$, as depicted in Figure 1 b. For these values of H, $D_-(H) \in (D_c, 1)$.

Ib. For $H \in (1/8, \frac{1}{2}(c+1))$, the component $\theta(t)$ is monotonic near the separatrix emanating from $D_-(H)$, as depicted in Figure 1 f. For these values of H, $D_-(H) \in (-1, 0)$.

II. $c < 0$

IIa. For $H \in (H_{\min}, -c/2)$, the component $\theta(t)$ is monotonic near the separatrix emanating from $D_+(H)$, as depicted in Figure 2 b,c. For these values of H, $D_+(H) \in (D_r, 1)$.

IIb. For $H \in (1/8, \frac{1}{2}(c+1))$, the component $\theta(t)$ is monotonic near the separatrix emanating from $D_-(H)$, as depicted in Figure 2 c,e. For these values of H, $D_-(H) \in (-1, 0)$.

ii. *Non monotonic θ dependence:* when $\frac{d\theta}{dt}$ changes sign along orbits in the vicinity of the separatrix (but not at the origin) the system is fully three dimensional on each energy surface. The methods developed by Wiggins[6] may be used to analyze the behavior of the separatrices. The geometrical interpretation of the results in terms of the transport in the four dimensional system is challenging. Such a behavior occurs in the following regimes:

I. $c > 0$:

Ic. For $H \in (H_c, 1/8)$, the component $\theta(t)$ is non-monotonic near the separatrix emanating from $D_-(H)$, as depicted in Figure 1 d,e. For these values of H, $D_-(H) \in (0, D_c)$.

II. $c < 0$

IIc. For $H \in (H_{\min}, 1/8)$, the component $\theta(t)$ is non-monotonic near the separatrix emanating from $D_-(H)$, as depicted in Figure 2 b,d. For these values of H, $D_-(H) \in (0, D_r)$.

Degenerate behavior

The interesting degenerate cases are listed below:

A. Hyperbolic resonance: When $\frac{d\theta}{dt}$ vanishes on the unstable fixed point $(\phi, v) = (0, 0)$, a strong resonance (1:1) occurs between the inertial trajectories and the forcing. Recent results by Kovacic and Wiggins and their extensions by Haller and Wiggins and Kaper and Kovacic[7] may be used to analyze this case. In these works the authors concentrated on finding criteria and proving theorems regarding the existence of transverse homoclinic orbits of various geometrical nature (analogously to finding the Melnikov integral in the one-and-a-half d.o.f. Hamiltonian systems). Such a behavior occurs in the following regime:

II. $-0.5 < c < 0$

IId. For $\epsilon = 0$ and $H = H_{\min}$, $\frac{d\theta}{dt} = 0$ at $D_-(H) = D_+(H) = D_r$, as depicted in Figure 2 b.

B. Behavior near Parabolic point: For $\epsilon > 0$ and all values of the other parameters, the behavior near the origin at $|D| = 1$ is mathematically non-trivial as it involves a perturbation of a parabolic point. It is expected to find exponentially small splitting of the separatrices near this point[8]. In terms of the energy surfaces, this region corresponds to the behavior near $H = H_{\min}$ and $H = H_{\max}$ where the energy surfaces change their topology.

C. Behavior on the $D = 0$ surface. For $\epsilon > 0$ and all values of the other parameters, the behavior near the separatrix for $D = 0$ is non-trivial, as, in the spherical coordinate system, in the limit $D \to 0$ the separatrices are discontinuous in v (reflecting the fact that v changes sign at the poles).

D. Zero wave speed. When $c = 0$, $\frac{d\theta}{dt} = 0$ at the elliptic fixed points $((\phi, v) = (\pm \arccos\sqrt{D}, 0))$, hence strong resonances are expected to occur along this surface. Moreover, since $D_r = D_c = 1$, these resonances end near $D = 1$ where a **parabolic resonance** appears.

E. Critical wave speed. When $c = -\frac{1}{2}$, the hyperbolic resonance (case IIb) occurs for $D_r = 0$, combining the two degenerate phenomena (A + C) which were discussed above.

4. Forcing with infinite wavelength ($k = 0$)

It follows from (2.9) that the (ϕ, v) system may be treated as a one-and-a-half d.o.f. Hamiltonian systems depending on the parameters D, σ and ϵ, and D may be taken to be positive as the (ϕ, v) system is invariant under $D \to -D$.

Interpretation in terms of the motion in the (λ, ϕ) has no such invariance; when $D < 0$ or $D > 1$ λ is monotonic in t, and when $0 < D < 1$, λ changes its direction when $\phi = \arccos\sqrt{D}$. In particular, the system (2.9) possesses a two dimensional surface of fixed points given by: $\{D, \lambda | (\phi, v, D, \lambda) = (\arccos\sqrt{D}, 0, D, \lambda), 0 \le D \le 1\}$. This situation is highly degenerate, especially at $D = 1$, hence additional perturbation, coupling the λ coordinate to the (ϕ, v) system (e.g. small k) is expected to cause strong resonances in addition to the $k = 0$ resonances discussed next.

Mathematically, one views the perturbed system as three dimensional in (ϕ, v, t) and considers the dynamics of the Poincaré map, a map found by sampling the solutions at $t = 2j\pi/\sigma + t_0$ for fixed t_0. For $D > 1$ the solutions to the unperturbed problem are periodic in t. In the Poincaré map, the orbits with periods which are rationally related to $2\pi/\sigma$ (these are called resonant orbits) appear as periodic orbits of the mapping, and those which are irrationally related trace a continuous curve. For small enough perturbation "most" of these curves survive (the ones which have periods sufficiently far from being resonant). When resonance of order n/m occurs, i.e., when the period of the periodic motion in the (ϕ, v) plane, $P_\phi(\phi_{\max}, D)$, satisfies:

$$P_\phi = \tfrac{n}{m}\tfrac{2\pi}{\sigma} \tag{4.1}$$

a chain of islands in the (ϕ, v) plane appears. Namely, a stable periodic orbit emerges, crossing the equator $2m$ times as t covers the interval $[0, 2n\pi/\sigma]$ and orbits which are sufficiently close to this solution - namely belong to the resonance band - oscillate about it (the width of the resonance band is proportional to $\sqrt{\epsilon}$ and is exponentially decreasing with n/m). It follows that strong resonances near the elliptic points occur when $\sigma \to 0$ near $|D| = 1$ and as $\sigma \to 1$ near $D = 0$. The latter limit is especially interesting as the elliptic points approach the separatrices as $D \to 0$.

For $|D| < 1$ the separatrix breaks down enabling orbits to spend several rounds in the north hemisphere and then hop to the south hemisphere and vice versa. The breakup of the separatrix is quantified by calculating the distance between the stable and unstable manifolds of the fixed point $(\phi, v, D) = (0, 0, \cos\phi_{hmax})$ along the ϕ-axis. In the Poincaré map $t = t_0$ this distance is given by:

$$d(t_0; \sigma, \phi_{hmax}) = \epsilon \frac{8M(t_0; \sigma, \phi_{hmax})}{|\sin(2\phi_{hmax})(1 - \frac{1}{\cos^2\phi_{hmax}})|} + O(\epsilon^2) \tag{4.2}$$

Where $M(t_0; \sigma, \phi_{hmax})$ is the Melnikov function[9,5], a periodic function in t of period $T = 2\pi/\sigma$:

$$M(t_0; \sigma, \phi_{hmax}) = 2\cos(\sigma t_0) \int_0^\infty vA'(\phi)\sin(\sigma t)\Big|_{q_s(t)} dt = M_0(\sigma, \phi_{hmax})\cos(\sigma t_0). \tag{4.3}$$

As long as $M_0(\sigma, \phi_{hmax})$ does not vanish the Melnikov function has simple zeroes, and the stable and unstable manifolds intersect transversely. It is customary to present the amplitude of the Melnikov function, $M_0(\sigma, \phi_{hmax})$. However, the normalization factor in (4.2) reflects the changes of the vector field on the homoclinic loop with ϕ_{hmax}, hence **a true measure to the size of the chaotic zone must include this factor**. Moreover, this factor changes the nature of the dependence on ϕ_{hmax} as $M_0(\sigma, \phi_{hmax})$ is monotonically increasing with ϕ_{hmax} whereas the maximal distance, $d(\sigma, \phi_{hmax})$ is not. In fact d attains a global maxima at $\phi_{hmax} \approx 0.4, \sigma \approx 0.25$. As σ is increased the "maximal chaos latitude" slightly increases as well. The width of the stochastic layer is monotonically increasing with $d(\sigma, \phi_{hmax})$ (though not linearly), hence its magnitude measures, roughly, the extent of the chaotic region.

The most rapid mixing between states bounded to one hemisphere and states visiting both hemispheres occurs when the flux per unit time, given by the lobe area[10] divided by the period, normalized by the homoclinic loop area is maximal:

$$\begin{aligned} F(\sigma, \phi_{hmax}) &= \frac{\text{Lobe area}}{\text{period} \cdot \text{homoclinic loop area}} \\ &= \frac{2|M_0(\sigma,\phi_{hmax})|/\sigma}{\frac{2\pi}{\sigma}\mu(R_1)} = \frac{|M_0(\sigma,\phi_{hmax})|}{\pi(\sin\phi_{hmax} - \phi_{hmax}\cos\phi_{hmax})} . \end{aligned} \tag{4.4}$$

Computing this function, we find that $F(\sigma, \phi_{hmax})$ attains its maxima at $\sigma \approx 0.25$ and $\phi_{hmax} \approx 0.5$. Hence the most rapid exchange of bounded to unbounded motion occurs for these values. To obtain more accurate estimates of the transport rates between the North and South hemisphere, the TAM may be employed[11].

5. Summary

Using the angular momentum and the Hamiltonian we have constructed energy surfaces, colored according to the zonal direction of propagation. This construction enabled us to classify readily the different regions in phase space in which the behavior is qualitatively different. In this initial study we have discussed the behavior in one particular case of infinite wavelength perturbation. For a fixed small strength of the pressure wave, we have identified the parameters and latitudes for which the chaotic zone is maximal and the values for which the mixing is most intense. The application of these results to observations on the dispersal of passive particles in the atmosphere and ocean is left for a sequel study.

Acknowledgement

The authors are indebted to Drs. M. Engel and A. Sigalov of the Center for Visualization of Dynamic Systems of the Hebrew University of Jeruslaem for their assistance in producing the figures contained in this paper. V. Rom-Kedar thanks for the hospitality of the Mathematics department of the University Of Chicago where part of this work has been carried out.

References

[1] W. Von-Arx [1974]. *An Introduction to Physical Oceanography.* Addison-Wesley Publishing Company Inc., Massachusetts.

[2] N. Paldor and P.D. Killworth [1988] Inertial Trajectories on a Rotating Earth, J. Atm. Sc., Vol. , No. 24, pp 4013-4019.

[3] N. Paldor and E. Boss [1992] Chaotic Trajectories of Tidally Perturbed Inertial Oscillations, J. Atm. Sc., Vol 49, 23, pp 2306-2318.

[4] E. Knobloch and J.B. Weiss, [1987], Mass Transport and Mixing by Modulated Traveling Waves. Phys. Rev. A, **36**, 1522, observed non-diffusive decay of autocorrelator. See Zaslavsky et al., this procceding, for the role of Lèvy flights in this process and for other references.

[5] See review and reference in J. Guckenheimer and P. Holmes [1983]. *Non-Linear Oscillations, Dynamical Systems and Bifurcations of Vector Fields.* Springer-Verlag, New York.

[6] S. Wiggins [1990]. *Introduction to Applied Nonlinear Dynamical Systems and Chaos.* Springer-Verlag: New York, Heidelberg, Berlin.

[7] G. Kovacic and S. Wiggins [1992] Orbits Homoclinic to resonances, with an application to chaos in a model of the forced and damped sine-Gordon equation, Physica D, 57 pp 185-225, G. Haller and S. Wiggins [1993] Orbits Homoclinic to resonances: the Hamiltonian case, Physica D, 66 pp 298-346, G. Haller and S. Wiggins [1994] N-pulse homoclinic orbits in perturbations of resonant Hamiltonian systems, to appear in Arch. of rational Mech., T. Kaper and G. Kovacic [1994] Multi-bump orbits homoclinic to resonance bands, preprint.

[8] P. Holmes, J. Marsden and J. Scheurle [1983] Exponentially small Splittings of Separatices with applications to KAM theory and Degenerate Bifurcations, Cont. Math. **81**, 213-244.

[9] V.K. Melnikov [1963] *On the Stability of the Center for Time Periodic Perturbations*, Trans. Moscow Math. Soc., **12**, 1.

[10] V. Rom-Kedar, A. Leonard and S. Wiggins [1990] An Analytical Study of Transport, Mixing and Chaos in an Unsteady Vortical Flow, JFM, vol. 214, pp. 347-394.

[11] V. Rom-Kedar [1994] Homoclinic Tangles - Classification and Applications, Nonlinearity, 7, 441-473.